

# Phase transitions in quantum dot-Majorana zero mode coupling systems

Yue Mao<sup>1</sup> and Qing-Feng Sun<sup>1, 2\*</sup>

<sup>1</sup> International Center for Quantum Materials, School of Physics, Peking University, 100871 Beijing, China

<sup>2</sup> Hefei National Laboratory, Hefei, 230088 Anhui, China

\* [sunqf@pku.edu.cn](mailto:sunqf@pku.edu.cn)

## Abstract

The magnetic doublet ground state (GS) of a quantum dot (QD) could be changed to a spin-singlet GS by coupling to a superconductor. In analogy, here we study the GS phase transitions in QD-Majorana zero mode (MZM) coupling systems: GS behaves phase transition versus intra-dot energy level and QD-MZM coupling strength. The phase diagrams of GS are obtained, for cases with and without Zeeman term. Along with the phase transition, we also study the change of spin feature and density of states. The properties of the phase transition are understood via a mean-field picture. Our study not only serves as an analogue to QD-superconductor phase transitions, but also gives alternative explanations on MZM-relevant experiments.

Copyright attribution to authors.

This work is a submission to SciPost Physics.

License information to appear upon publication.

Publication information to appear upon publication.

Received Date

Accepted Date

Published Date

1

## 2 Contents

3	<b>1 Introduction</b>	2
4	<b>2 Model and formula</b>	3
5	<b>3 Phase transition without Zeeman term</b>	6
6	<b>4 Phase transition with Zeeman term</b>	9
7	<b>5 Conclusion</b>	13
8	<b>A The role of normal lead</b>	13
9	<b>References</b>	14

10

11

## 1 Introduction

When a quantum dot (QD) couples to a BCS-type superconductor, rich physical contents emerge in the quantum phase transition of the QD [1–7]. By controlling the intra-dot energy level, the QD itself could exhibit two kinds of ground states (GSs): a magnetic doublet state and a spin singlet state. The doublet state represents two degenerate spin- $\hbar/2$  states, a spin-up state  $|\uparrow\rangle$  and a spin-down state  $|\downarrow\rangle$ . The QD is occupied by one electron, while the level with opposite spin is repulsed above Fermi surface by the Coulomb interaction and is empty. The singlet state originates from spinless states  $|0\rangle$  and  $\frac{1}{\sqrt{2}}(|\uparrow\downarrow\rangle - |\downarrow\uparrow\rangle)$ , with zero and two electrons occupied, respectively. When coupled to a superconductor, the doublet state of the QD could be changed to a singlet state either by the proximity effect of spin-singlet Cooper pairs or by coupling to the quasiparticles outside the gap [6, 8–10]. Whether the GS is doublet or singlet is mostly determined by the charging energy, the intra-dot energy level, and the coupling strength [2–7, 11, 12]. This doublet-singlet phase transition plays an important role in properties of the QD-superconductor hybrid devices, such as  $0 - \pi$  transition of Josephson junctions [1, 13, 14] and level crossing of Andreev bound states [2–6].

In certain superconducting systems, there could exist a special Andreev bound state called Majorana zero mode (MZM), which is its own antiparticle [8, 9, 15–37]. MZM is a hotspot in condensed matter physics because of its non-Abelian statistics, which can be managed to achieve fault-tolerated topological quantum computation [38–41]. Like a superconductor, the MZM also couples to electron and hole simultaneously [42]. Especially, because of its self-Hermitian property, the half fermionic MZM couples to a certain spin channel, leading to the resonant equal-spin Andreev reflection [26, 27, 29, 43, 44]. The MZM thus behaves strong spin-triplet pairing correlations [44, 45], and induces a zero bias peak spectrum in both charge transport and spin-dependent transport [42, 43, 46].

In platforms for generating MZMs, Coulomb interaction could play an important role by influencing the Andreev bound states [4, 6, 9, 21, 24–27]. In particular, a QD region can be formed nearby the MZM, e.g. by an adatom deposited on the iron-based superconductor [9, 47] or by a section of the Majorana nanowire [4–6, 21]. The QD-MZM coupling system can be regarded as a counterpart to the QD-superconductor hybrid structure, because the MZM is an Andreev bound state generated by the superconductor. But differently, the coupling term between the QD and the MZM involves only one spin channel, destroying the spin rotation symmetry. Compared to coupling with a conventional superconductor, does phase transition also happen in QD-MZM coupling systems? Will the peculiar features of the MZM lead to novel transition characteristics?

In this paper, we study the QD-MZM coupling system and find the corresponding phase transitions. Because spin rotation symmetry is broken, the degeneracy of the magnetic doublet state is destroyed, with GS becoming a spin-polarized state. By changing the intra-dot energy level and coupling strength, phase transition of GS happens with spin reversed. We study two cases without and with Zeeman term (which should be included considering experimental conditions), and give global phase diagrams showing the phase transition lines. These phase transitions influence occupation numbers, spin polarization, density of states (DOS), and the weight of zero energy state. These features are explained by a mean-field picture. Our theoretical results are also discussed by comparing with experimental observations. These phase transitions can provide an insight on MZM-related transport experiments.

The rest of this paper is as follows: In Sec. 2, the model and formula of the system are given. In Sec. 3, we study the phase transitions without Zeeman term. In Sec. 4, we consider the Zeeman term and study the corresponding phase transitions. At last, a brief conclusion is given in Sec. 5. In Appendix A, we explain the role of normal lead in detail.

## 2 Model and formula

As shown in Fig. 1, the system we study consists of a QD coupled to a MZM and a normal lead. The total Hamiltonian is

$$H = H_D + H_{DM} + H_{ND} + H_N. \quad (1)$$

Here  $H_D$ ,  $H_{DM}$ ,  $H_{ND}$ , and  $H_N$  respectively represent the QD, the coupling between QD and MZM, the coupling between QD and normal lead, and the normal lead [42, 43, 46, 48, 49]:

$$H_D = (\epsilon_0 - V_Z)d_\uparrow^\dagger d_\uparrow + (\epsilon_0 + V_Z)d_\downarrow^\dagger d_\downarrow + Un_\uparrow n_\downarrow, \quad (2)$$

$$H_{DM} = it(d_\uparrow + d_\uparrow^\dagger)\gamma, \quad (3)$$

$$H_{ND} = \sum_{k\sigma} t_N c_{k\sigma}^\dagger d_\sigma + h.c., \quad (4)$$

$$H_N = \sum_{k\sigma} \epsilon_k c_{k\sigma}^\dagger c_{k\sigma}, \quad (5)$$

where  $d_\sigma$  and  $c_{k\sigma}$  are annihilation operators of electrons in QD and normal lead, respectively, with spin  $\sigma = \uparrow, \downarrow$ .  $\epsilon_0$  is the intra-dot energy level of the QD.  $t_N$  is the hopping strength between the normal lead and the QD. The electron-electron interaction is included in  $H_D$  as the term  $Un_\uparrow n_\downarrow$ , with  $U$  the charging energy and  $n_\sigma = d_\sigma^\dagger d_\sigma$  the particle number operator [1, 4, 6, 50–54]. In our calculations, we always set  $U = 1$  as the energy unit.  $\gamma$  is the operator of the MZM. The MZMs always emerge in pair, and their coupling strength is determined by the overlap of their wavefunctions [16, 22, 48]. Their nonlocality relates to separation between a pair of MZMs, which can be measured also through the normal lead-QD-MZM systems [22, 55]. In our study, we consider the pair of MZMs are well separated (e.g. as long as the Majorana nanowire is long). They are almost decoupled and only one MZM  $\gamma$  couples to the QD [42, 43]. The generation of MZM usually demands the existence of a conventional superconductor, which is not included in our model. This is because we focus on the MZM at zero energy, where the DOS is not affected by the superconducting continuum outside the gap. Also, this is to provide a concise comparison to QD-superconductor systems.

In order to regulate the topological superconductor to the nontrivial phase, a magnetic term, such as an external magnetic field [18, 19] or magnetic exchange coupling of QD [8, 9], is usually demanded. Therefore, the QD inevitably feels a Zeeman energy  $V_Z$ , which here represents the effective magnetic field parallel to the spin-up direction. Due to the self-Hermitian property  $\gamma^\dagger = \gamma$ , the MZM couples to electrons and holes with the same strength  $t$  [42], and only one spin channel is coupled [43]. Inducing the MZM usually demands a large Zeeman term  $-V_Z\sigma_z$ , and in this case the MZM almost just couples to spin  $+z$  [22, 43, 44]. This corresponds to Eq. (3) where  $\gamma$  is just coupled to the  $d_\uparrow$  channel. Note that there are only two spin-dependent terms in the Hamiltonian: the Zeeman term and the MZM-QD coupling. Even if  $V_Z$  is not large and the MZM couples to both  $+z$  and  $-z$  spin  $ad_z + bd_{\bar{z}}$  ( $a, b$  are normalized coefficients), one can rotate the spin basis as  $d_\uparrow = ad_z + bd_{\bar{z}}$ . In this new basis, the MZM still only couples to  $d_\uparrow$ , and the spin direction of the Zeeman term is a bit deviated from  $\uparrow$  spin direction. If  $V_Z = 0$  and the Zeeman term is absent, setting that MZM just couples to  $d_\uparrow$  has no influence on any other term of the Hamiltonian. Therefore, it is reasonable to set that the MZM couples to electrons and holes of spin-up channel, as shown in Eq. (3).

In fact, when the normal lead is decoupled, the system can be exactly solved by diagonalization. Here we consider the normal lead coupled to the QD, because (i) a lead is usually needed to probe the existence of MZMs in experiments and (ii) the normal lead can facilitate the visualization of DOS by directly providing a broadening via the imaginary parts of retarded Green's functions. This broadening is important to reflect the MZM signal change along with

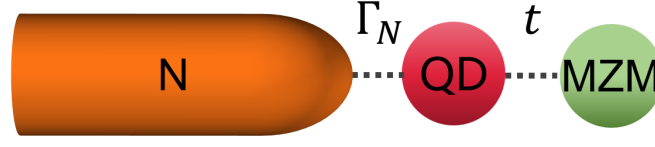


Figure 1: The schematic plot for the QD-MZM coupling system. In addition, the QD is weakly coupled to a normal lead, for the visualization of DOS and a better description of practical experiments.  $\Gamma_N$  and  $t$  respectively indicate the strength of QD-normal lead coupling and QD-MZM coupling.

99 the phase transition, as explained in Appendix A. The normal lead-QD coupling is  
 100 described by  $\Gamma_N = \pi\rho_N t_N^2$  with  $\rho_N$  the DOS in the normal lead [46]. In normal lead-QD-  
 101 MZM systems, there is also the Kondo effect, which has been studied by researchers [56, 57].  
 102 It corresponds to the case that the temperature  $T$  is comparable to the Kondo temperature  
 103  $T_K$ . Below we set a weak normal lead-QD coupling with  $\Gamma_N = 0.01U$ . What is more, be-  
 104 cause the coupling between QD and normal lead is weak, the Kondo temperature  $T_K$  is very  
 105 low [58], and the condition  $T \gg T_K$  is easily met, thus our study is not relevant to the Kondo  
 106 regime [56, 57, 59–61].

107 Below we first diagonalize the system without normal lead to obtain the GS. By doing this,  
 108 the energy level and occupation numbers  $\langle n_\sigma \rangle$  are exactly solved, and the phase transitions  
 109 are revealed. Based on the GS, we introduce the normal lead as the imaginary part of Green's  
 110 function, so that the DOS has a broadening and can be visualized. We represent the MZM by  
 111 the normal Fermion operator  $\gamma = \frac{1}{\sqrt{2}}(c + c^\dagger)$ .

112 When the normal lead is absent, there exist four possible occupations of the QD, and two  
 113 possible occupations of the MZM system. Therefore, the Hamiltonian can be written as a  $8 \times 8$   
 114 matrix, in the basis  $(|0, 0, 0\rangle, |1, 1, 0\rangle, |1, 0, 0\rangle, |0, 1, 0\rangle, |0, 0, 1\rangle, |1, 1, 1\rangle, |1, 0, 1\rangle, |0, 1, 1\rangle)$ . Here

$$|i, j, k\rangle = |n_c = i, n_\uparrow = j, n_\downarrow = k\rangle = (c^\dagger)^i (d_\uparrow^\dagger)^j (d_\downarrow^\dagger)^k |0\rangle. \quad (6)$$

115 The Hamiltonian has four  $2 \times 2$  blocks  $H_1 \oplus H_2 \oplus H_3 \oplus H_4$ , with

$$H_1 = \begin{pmatrix} 0 & \frac{it}{\sqrt{2}} \\ \frac{-it}{\sqrt{2}} & \epsilon_0 - V_Z \end{pmatrix}, \quad H_2 = \begin{pmatrix} 0 & \frac{-it}{\sqrt{2}} \\ \frac{it}{\sqrt{2}} & \epsilon_0 - V_Z \end{pmatrix}, \quad (7)$$

$$H_3 = \begin{pmatrix} \epsilon_0 + V_Z & \frac{it}{\sqrt{2}} \\ \frac{-it}{\sqrt{2}} & 2\epsilon_0 + U \end{pmatrix}, \quad H_4 = \begin{pmatrix} \epsilon_0 + V_Z & \frac{-it}{\sqrt{2}} \\ \frac{it}{\sqrt{2}} & 2\epsilon_0 + U \end{pmatrix}. \quad (8)$$

116 The four blocks correspond to eight eigenvalues

$$\epsilon_{1,\pm} = \epsilon_{2,\pm} = \frac{\epsilon_0 - V_Z \pm \sqrt{(\epsilon_0 - V_Z)^2 + 2t^2}}{2}, \quad (9)$$

$$\epsilon_{3,\pm} = \epsilon_{4,\pm} = \frac{3\epsilon_0 + U + V_Z \pm \sqrt{(\epsilon_0 + U - V_Z)^2 + 2t^2}}{2}. \quad (10)$$

117 Focusing on the occupation of the QD, we can find that  $H_1, H_2$  both correspond to basis  
 118  $(|n_\uparrow = 0, n_\downarrow = 0\rangle, |n_\uparrow = 1, n_\downarrow = 0\rangle)$ , and  $H_3, H_4$  both correspond to basis  $(|n_\uparrow = 0, n_\downarrow = 1\rangle, |n_\uparrow = 1, n_\downarrow = 1\rangle)$ .  
 119 What is more, because  $H_1 = H_2^*, H_3 = H_4^*$ , their eigenvectors satisfy  $\psi_{1,\pm} = \psi_{2,\pm}^*, \psi_{3,\pm} = \psi_{4,\pm}^*$ .  
 120 For the above reasons,  $\psi_{1,\pm}$  and  $\psi_{2,\pm}$  ( $\psi_{3,\pm}$  and  $\psi_{4,\pm}$ ), the degenerate eigenstates of  $H_1$  and  
 121  $H_2$  ( $H_3$  and  $H_4$ ), have the same occupations of the QD and indicate spin-up (spin-down) states.  
 122 Thus, we can just analyze  $H_1$  and  $H_3$  only.

123 The GS energy can only equal to  $\epsilon_{1,-}$  or  $\epsilon_{3,-}$ . The GS is judged by the sign of  $\epsilon_{3,-} - \epsilon_{1,-}$ .  
 124 For  $\epsilon_{1,-} < \epsilon_{3,-}$ , the GS energy is  $\epsilon_{1,-}$ , and its occupation numbers can be obtained from  $\psi_{1,-}$   
 125 for Hamiltonian  $H_1$

$$\langle n_\uparrow \rangle = \frac{1}{2} \left( 1 - \frac{\epsilon_0 - V_Z}{\sqrt{(\epsilon_0 - V_Z)^2 + 2t^2}} \right), \quad \langle n_\downarrow \rangle = 0. \quad (11)$$

126 Because  $\langle n_\downarrow \rangle = 0$ , the state of the QD is spin-up and contributed by  $|0\rangle$  and  $|\uparrow\rangle$ . For  $\epsilon_{1,-} > \epsilon_{3,-}$ ,  
 127 the GS energy is  $\epsilon_{3,-}$ , and its occupation numbers can be obtained from  $\psi_{3,-}$  for Hamiltonian  
 128  $H_3$

$$\langle n_\uparrow \rangle = \frac{1}{2} \left( 1 - \frac{\epsilon_0 + U - V_Z}{\sqrt{(\epsilon_0 + U - V_Z)^2 + 2t^2}} \right), \quad \langle n_\downarrow \rangle = 1. \quad (12)$$

129 Because  $\langle n_\downarrow \rangle = 1$ , the state is spin-down and contributed by  $|\downarrow\rangle$  and  $\frac{1}{\sqrt{2}}(|\uparrow\downarrow\rangle - |\downarrow\uparrow\rangle)$ . When  
 130 the parameters change, the sign of  $\epsilon_{3,-} - \epsilon_{1,-}$  can also change and result in the GS transition  
 131 between  $\psi_{1,-}$  and  $\psi_{3,-}$ .

132 Next we solve the single-particle DOS from retarded Green's function. The single particle  
 133 can be electron  $e\sigma$  or hole  $h\sigma$ , with spin  $\sigma = \uparrow, \downarrow$ . The energy space Green's function is obtained  
 134 from the time space via **Fourier** transformation

$$G_{D,e(h)\sigma e(h)\sigma}^r(\epsilon) = \int dt e^{i\epsilon t} G_{D,e(h)\sigma e(h)\sigma}^r(t). \quad (13)$$

135 The time-space Green's function of  $e\sigma$  is

$$\begin{aligned} G_{D,e\sigma e\sigma}^r(t) &= -i\theta(t) \langle g|d_\sigma(t)d_\sigma^\dagger(0) + d_\sigma^\dagger(0)d_\sigma(t)|g\rangle \\ &= -i\theta(t) \sum_j [\langle g|d_\sigma(t)|j\rangle \langle j|d_\sigma^\dagger(0)|g\rangle + \langle g|d_\sigma^\dagger(0)|j\rangle \langle j|d_\sigma(t)|g\rangle] \\ &= -i\theta(t) \sum_j [e^{i(\epsilon_g - \epsilon_j)t} \langle g|d_\sigma(0)|j\rangle \langle j|d_\sigma^\dagger(0)|g\rangle + e^{i(\epsilon_j - \epsilon_g)t} \langle g|d_\sigma^\dagger(0)|j\rangle \langle j|d_\sigma(0)|g\rangle] \\ &= -i\theta(t) \sum_j [e^{i(\epsilon_g - \epsilon_j)t} |\tilde{A}_\sigma(g, j)|^2 + e^{i(\epsilon_j - \epsilon_g)t} |\tilde{A}_\sigma(j, g)|^2]. \end{aligned} \quad (14)$$

136 Here we use the eigenstate basis  $j = 1, 2, 3, \dots, 8$  corresponding to  $\psi_{1,-}, \psi_{1,+}, \psi_{2,-}, \dots, \psi_{4,+}$ .  
 137  $g$  indicates the order number  $j$  of GS. When  $\epsilon_{1,-} < \epsilon_{3,-}$  ( $\epsilon_{1,-} > \epsilon_{3,-}$ ),  $g = 1$  ( $g = 5$ ) indi-  
 138 cates  $\psi_{1,-}$  ( $\psi_{3,-}$ ). Note that the term  $\langle g|d_\sigma(t)|j\rangle$  is in the Heisenberg representation and can  
 139 be transformed to Schrödinger representation  $\langle g(t)|d_\sigma(0)|j(t)\rangle = e^{i(\epsilon_g - \epsilon_j)t} \langle g|d_\sigma(0)|j\rangle$ . Simi-  
 140 larly, we get  $\langle j|d_\sigma(t)|g\rangle = e^{i(\epsilon_j - \epsilon_g)t} \langle j|d_\sigma(0)|g\rangle$ .  $\tilde{A}_\sigma(x, y) = \langle x|d_\sigma(0)|y\rangle$  is the representation  
 141 of  $d_\sigma(0)$  in the  $j$  basis. It is obtained by a unitary transformation on  $A_\sigma$ , which is the represen-  
 142 tation of  $d_\sigma(0)$  in the basis of  $H_1$  to  $H_4$  (basis Eq. (6)):  $A_\uparrow$  is a  $8 \times 8$  matrix with four nonzero  
 143 elements  $A_\uparrow(1, 4) = A_\uparrow(5, 8) = 1$ ,  $A_\uparrow(3, 2) = A_\uparrow(7, 6) = -1$ .  $A_\downarrow$  is also a  $8 \times 8$  matrix with four  
 144 nonzero elements  $A_\downarrow(1, 5) = A_\downarrow(2, 6) = 1$ ,  $A_\downarrow(3, 7) = A_\downarrow(4, 8) = -1$ . The transformation is

145  $\tilde{A}_\sigma = V^\dagger A_\sigma V$ , with  $V = V_1 \oplus V_2 \oplus V_3 \oplus V_4$  obtained from the eigenvectors of  $H_1$  to  $H_4$ :

$$V_1 = \begin{pmatrix} \frac{it}{\sqrt{t^2+2\epsilon_{1,-}^2}} & \frac{it}{\sqrt{t^2+2\epsilon_{1,+}^2}} \\ \frac{\sqrt{2}\epsilon_{1,-}}{\sqrt{t^2+2\epsilon_{1,-}^2}} & \frac{\sqrt{2}\epsilon_{1,+}}{\sqrt{t^2+2\epsilon_{1,+}^2}} \end{pmatrix}, \quad (15)$$

$$V_2 = \begin{pmatrix} \frac{-it}{\sqrt{t^2+2\epsilon_{1,-}^2}} & \frac{-it}{\sqrt{t^2+2\epsilon_{1,+}^2}} \\ \frac{\sqrt{2}\epsilon_{1,-}}{\sqrt{t^2+2\epsilon_{1,-}^2}} & \frac{\sqrt{2}\epsilon_{1,+}}{\sqrt{t^2+2\epsilon_{1,+}^2}} \end{pmatrix}, \quad (16)$$

$$V_3 = \begin{pmatrix} \frac{it}{\sqrt{t^2+2(\epsilon_{3,-}-\epsilon_0-V_Z)^2}} & \frac{it}{\sqrt{t^2+2(\epsilon_{3,+}-\epsilon_0-V_Z)^2}} \\ \frac{\sqrt{2}(\epsilon_{3,-}-\epsilon_0-V_Z)}{\sqrt{t^2+2(\epsilon_{3,-}-\epsilon_0-V_Z)^2}} & \frac{\sqrt{2}(\epsilon_{3,+}-\epsilon_0-V_Z)}{\sqrt{t^2+2(\epsilon_{3,+}-\epsilon_0-V_Z)^2}} \end{pmatrix}, \quad (17)$$

$$V_4 = \begin{pmatrix} \frac{-it}{\sqrt{t^2+2(\epsilon_{3,-}-\epsilon_0-V_Z)^2}} & \frac{-it}{\sqrt{t^2+2(\epsilon_{3,+}-\epsilon_0-V_Z)^2}} \\ \frac{\sqrt{2}(\epsilon_{3,-}-\epsilon_0-V_Z)}{\sqrt{t^2+2(\epsilon_{3,-}-\epsilon_0-V_Z)^2}} & \frac{\sqrt{2}(\epsilon_{3,+}-\epsilon_0-V_Z)}{\sqrt{t^2+2(\epsilon_{3,+}-\epsilon_0-V_Z)^2}} \end{pmatrix}. \quad (18)$$

146 From the process above,  $\tilde{A}_\sigma$  and  $G_{D,e\sigma e\sigma}^r(t)$  are solved, and  $G_{D,e\sigma e\sigma}^r(\epsilon)$  is obtained via Eq. (13)

147

$$G_{D,e\sigma e\sigma}^r(\epsilon) = \sum_j \left[ \frac{|\tilde{A}_\sigma(g, j)|^2}{\epsilon - \epsilon_j + \epsilon_g + i\Gamma_N} + \frac{|\tilde{A}_\sigma(j, g)|^2}{\epsilon - \epsilon_g + \epsilon_j + i\Gamma_N} \right]. \quad (19)$$

148 Here, the coupling of normal lead is included as the imaginary part  $\Gamma_N = \pi\rho_N t_N^2 = 0.01U$  [46].

149 Similarly,  $G_{D,h\sigma h\sigma}^r(\epsilon)$  can be solved by substituting  $d_\sigma$  by  $d_\sigma^\dagger$  in Eq. (14), and is equivalent to

150 substituting  $\tilde{A}_\sigma$  by  $\tilde{A}_\sigma^\dagger$  in Eq. (19). The single-particle DOS is obtained from the retarded

151 Green's function [4]

$$\rho_{e(h)\sigma}(\epsilon) = -\frac{1}{\pi} \text{Im}[G_{D,e(h)\sigma e(h)\sigma}^r(\epsilon)]. \quad (20)$$

### 152 3 Phase transition without Zeeman term

153 First we consider a simple case that the Zeeman term  $V_Z = 0$ . When the QD-MZM coupling  
154 strength  $t = 0$ , the result returns to that of an isolated QD [4–7, 11, 12]: The QD has a degener-  
155 erate doublet GS in the range  $-U < \epsilon_0 < 0$ , while the GS is singlet outside this region. The  
156 physics we most concern with is how the doublet state of QD is influenced by the MZM, i.e. the  
157 case  $-U < \epsilon_0 < 0$ . When the MZM is not coupled to the QD ( $t = 0$ ), the spin rotation symme-  
158 try leads to the doublet state: With the total occupation number being 1, the two degenerate  
159 states  $|\uparrow\rangle$  and  $|\downarrow\rangle$  are respectively occupied by just a spin-up electron and just a spin-down  
160 electron. The GS can be either  $|\uparrow\rangle$  with  $\langle n_\uparrow \rangle = 1, \langle n_\downarrow \rangle = 0$  or  $|\downarrow\rangle$  with  $\langle n_\uparrow \rangle = 0, \langle n_\downarrow \rangle = 1$ .

161 The MZM only couples to spin-up channel with strength  $t$ , causing the broken spin rota-  
162 tion symmetry and broken degeneracy of doublet state. According to Eqs. (11,12), the two  
163 eigenstates  $\psi_{1,-}, \psi_{3,-}$  consist of both spin-up and spin-down occupation. They are respectively  
164 dominated by spin-up and spin-down components, and can be respectively called spin-up state  
165 and spin-down state.

166 On this condition, the energies of spin-up state and spin-down state  $\epsilon_{1,-}, \epsilon_{3,-}$  are different,  
167 and the GS is determined by the sign of

$$\begin{aligned} \epsilon_{3,-} - \epsilon_{1,-} &= \frac{1}{2} \left[ 2\epsilon_0 + U + \sqrt{\epsilon_0^2 + 2t^2} - \sqrt{(\epsilon_0 + U)^2 + 2t^2} \right] \\ &= \frac{2\epsilon_0 + U}{2} \left[ 1 - \frac{U}{\sqrt{\epsilon_0^2 + 2t^2} + \sqrt{(\epsilon_0 + U)^2 + 2t^2}} \right]. \end{aligned} \quad (21)$$

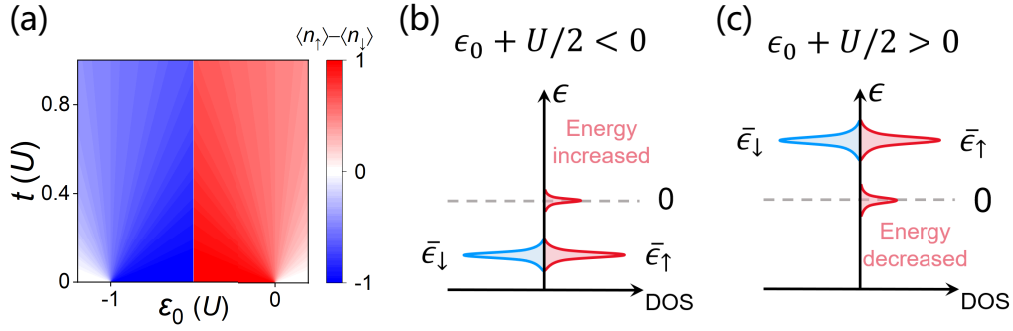


Figure 2: (a) The phase diagram versus intra-dot energy level  $\epsilon_0$  and MZM coupling strength  $t$  for  $V_Z = 0$ . Here we plot  $\langle n_\uparrow \rangle - \langle n_\downarrow \rangle$  to show the spin polarization. (b, c) The mean-field picture for the phase transition. Without the coupling of MZM, spin  $\uparrow$  and  $\downarrow$  have the same average energy level  $\bar{\epsilon}_\uparrow = \bar{\epsilon}_\downarrow = \epsilon_0 + U/2$ . The leakage of MZM induces a zero-energy peak in spin- $\uparrow$  channel. Thus, the spin- $\uparrow$  energy is effectively increased (decreased) for  $\epsilon_0 + U/2 < 0$  ( $\epsilon_0 + U/2 > 0$ ), corresponding to a spin-down (spin-up) GS.

168 Note that when  $t \neq 0$ ,  $\sqrt{\epsilon_0^2 + 2t^2} + \sqrt{(\epsilon_0 + U)^2 + 2t^2} > U$ , and  $1 - \frac{U}{\sqrt{\epsilon_0^2 + 2t^2} + \sqrt{(\epsilon_0 + U)^2 + 2t^2}} > 0$ .

169 Therefore, the sign of  $\epsilon_{3,-} - \epsilon_{1,-}$  is determined by the sign of  $2\epsilon_0 + U$ . When  $\epsilon_0 < -U/2$   
 170 ( $\epsilon_0 > -U/2$ ),  $\epsilon_{3,-} < \epsilon_{1,-}$  ( $\epsilon_{3,-} > \epsilon_{1,-}$ ), the GS is the spin-down state  $\psi_{3,-}$  (spin-up state  $\psi_{1,-}$ ).  
 171 As shown in Fig. 2(a), we calculate and compare the energy  $\epsilon_{1,-}$ ,  $\epsilon_{3,-}$ , so that we judge which  
 172 is the GS. Then the spin of GS  $\langle n_\uparrow \rangle - \langle n_\downarrow \rangle$  is plotted in the  $\epsilon_0, t$  parameter space. A remarkable  
 173 signature is the phase transition at  $\epsilon_0 = -U/2$ , consistent with Eq. (21). Indeed, the GS is  
 174 **spin-down** for  $\epsilon_0 < -U/2$  and reversed to **spin-up** for  $\epsilon_0 > -U/2$ . The case is different from  
 175 coupling to conventional superconductor, where the doublet GS can be changed to spin-singlet  
 176 GS [4–7, 11, 12].

177 The phase transition can be understood by the single-particle effective energy levels in a  
 178 mean-field picture. Due to the intra-dot Coulomb repulsion  $Un_\uparrow n_\downarrow$ , the energy level of certain  
 179 spin is lifted from  $\epsilon_0$  by the filled electron with opposite spin: The spin-up and spin-down  
 180 occupations are determined by their spin-dependent effective energy levels  $\epsilon_\uparrow = \epsilon_0 + \langle n_\downarrow \rangle U$   
 181 and  $\epsilon_\downarrow = \epsilon_0 + \langle n_\uparrow \rangle U$ . Without coupling of MZM ( $t = 0$ ) and for doublet state ( $-U < \epsilon_0 < 0$ ),  
 182 the spin-up state  $|\uparrow\rangle$  corresponds to  $\langle n_\uparrow \rangle = 1$  and  $\langle n_\downarrow \rangle = 0$ , so  $\epsilon_\uparrow = \epsilon_0$  and  $\epsilon_\downarrow = \epsilon_0 + U$  are  
 183 respectively below and above the Fermi energy  $E_F = 0$ . Self-consistently, these spin-dependent  
 184 effective levels indicate occupation numbers  $\langle n_\uparrow \rangle = 1$  and  $\langle n_\downarrow \rangle = 0$  and that only spin-up  
 185 channel is occupied [1, 4, 6]. Similarly, the spin-down state  $|\downarrow\rangle$  corresponds to  $\epsilon_\uparrow = \epsilon_0 + U$  and  
 186  $\epsilon_\downarrow = \epsilon_0$ . The discussion and symbol  $\epsilon_\sigma$  above is based on that GS spin has been determined.  
 187 Before the GS is determined, we consider both cases of spin polarization and take the average.  
 188 The average energy levels are  $\bar{\epsilon}_\uparrow = \bar{\epsilon}_\downarrow = \epsilon_0 + U/2$ , as schematically shown in the two major  
 189 DOS peaks in Figs. 2(b, c). Therefore, the GS is degenerate doublet state  $|\uparrow\rangle$  and  $|\downarrow\rangle$ .

190 When MZM is coupled to QD with  $t \neq 0$ , the MZM leaks into the spin-up channel of the  
 191 QD [62], bringing an additional peak at zero energy [zero-energy peaks in Figs. 2(b, c)]. The  
 192 spin-up channel is initially located at  $\bar{\epsilon}_\uparrow$ , the MZM induced zero-energy peak effectively moves  
 193 its energy level close to 0. When  $\bar{\epsilon}_\uparrow = \bar{\epsilon}_\downarrow = \epsilon_0 + U/2 < 0$ , the effective energy level of spin  
 194 up is lifted to higher than  $\bar{\epsilon}_\downarrow$ , as shown in Fig. 2(b). The higher energy of the spin-up channel  
 195 indicates that the GS is the spin-down state  $\psi_{3,-}$ . On the other hand, for  $\epsilon_0 + U/2 > 0$ , the  
 196 spin-up energy is effectively reduced by MZM coupling, as shown in Fig. 2(c). Thus, the spin-  
 197 up channel has the lower energy than spin-down channel, and the GS is spin-up state  $\psi_{1,-}$ .  
 198 This picture explains the phase transition and spin change in Eq. (21) and Fig. 2(a).

199 In the presence of QD-MZM coupling  $t$ , the broken spin rotation symmetry not only de-

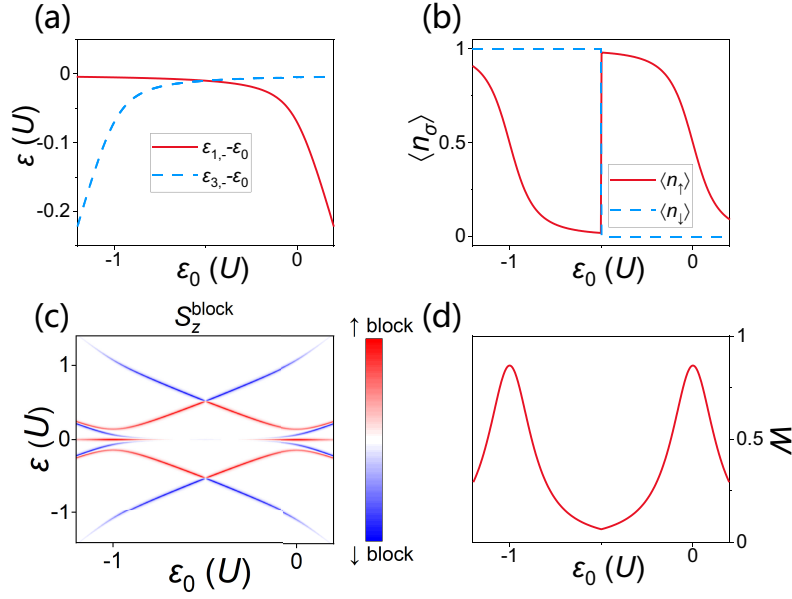


Figure 3: Phase transition of GS versus intra-dot energy level  $\epsilon_0$  for  $V_Z = 0$ . (a) Energy comparison of spin-up and spin-down states  $\epsilon_{1,-}$  and  $\epsilon_{3,-}$ .  $\epsilon_0$  is **subtracted** for clarity. (b) The occupation numbers  $\langle n_\uparrow \rangle$ ,  $\langle n_\downarrow \rangle$  of GS. (c) The spin-resolved single-particle DOS. (d) The weight of zero-energy spin-up DOS. In these figures (a-d), the QD-MZM coupling strength  $t = 0.1U$ .

200 stroy the degeneracy of doublet state for  $-U < \epsilon_0 < 0$ , but also transforms the initial spin-  
 201 singlet state for  $\epsilon_0 < -U$  or  $\epsilon_0 > 0$  to **become** spin polarized. In other words, the GS is  
 202 spin-polarized in the whole phase diagram [Fig. 2(a)], which is distinct from the doublet-  
 203 singlet phase diagram in spin-singlet superconductor-QD system [4–7, 11, 12]. In addition, if  
 204 the MZM is decoupled, the QD should be occupied by zero or two electrons when  $\epsilon_0 > 0$  or  
 205  $\epsilon_0 < -U$ , and the state should respectively be **the** spin-singlet  $|0\rangle$  or  $\frac{1}{\sqrt{2}}(|\uparrow\downarrow\rangle - |\downarrow\uparrow\rangle)$ . Thus,  
 206 the corresponding spin polarization is nearly zero for very small MZM coupling  $t$ .

207 We also investigate the features of GS phase transition versus the intra-dot energy level  
 208  $\epsilon_0$ . In experiments this  $\epsilon_0$  can be regulated by applying a gate voltage [4–6, 21]. The QD-  
 209 MZM coupling strength is fixed to be  $t = 0.1U$ . The energy comparison of states  $\psi_{1,-}, \psi_{3,-}$   
 210 is plotted in Fig. 3(a). Because  $\epsilon_{1,-}, \epsilon_{3,-}$  are both mainly proportional to  $\epsilon_0$ , the **energies**  
 211 are simultaneously subtracted by  $\epsilon_0$  in Fig. 3(a) for a clear comparison. Just as the Eq. (21)  
 212 and Fig. 2(a),  $\epsilon_{1,-} > \epsilon_{3,-}$  ( $\epsilon_{1,-} < \epsilon_{3,-}$ ) for  $\epsilon_0 + U/2 < 0$  ( $\epsilon_0 + U/2 > 0$ ), indicating the GS  
 213 is the spin-down (spin-up) state. Fig. 3(b) shows the occupation numbers  $\langle n_\uparrow \rangle, \langle n_\downarrow \rangle$  versus  
 214  $\epsilon_0$ . As  $\epsilon_0$  increases and crosses  $-U/2$  and phase transition happens, the spin polarization  
 215 of GS undergoes a sharp transition from  $\langle n_\downarrow \rangle = 1$  to  $\langle n_\downarrow \rangle = 0$ . In the mean-field picture,  
 216  $\epsilon_\uparrow = \epsilon_0 + \langle n_\downarrow \rangle U$  also changes from  $\epsilon_\uparrow = \epsilon_0 + U = 0.5U$  to  $\epsilon_\uparrow = \epsilon_0 - 0.5U$ . For  $\epsilon_\uparrow = 0.5U > 0$ ,  
 217 the spin-up channel is almost not occupied, with  $\langle n_\uparrow \rangle \approx 0$ . But for  $\epsilon_\uparrow = -0.5U < 0$ , the spin-up  
 218 channel is almost occupied, with  $\langle n_\uparrow \rangle \approx 1$ . On the other hand, the MZM-induced zero-energy  
 219 peak tends to move  $\langle n_\uparrow \rangle$  to 0.5, thus around  $\epsilon_0 = -U/2$ ,  $\langle n_\uparrow \rangle$  is a bit deviated from 0 or 1. The  
 220 lower  $|\epsilon_\uparrow|$  is, the more evident the MZM-induced zero-energy leakage. Because  $\epsilon_\uparrow = \pm U/2$  is  
 221 far from zero, the leakage effect is weak and  $\langle n_\uparrow \rangle$  is almost 0 or 1 around  $\epsilon_0 = -U/2$ . For the  
 222 two separated regions  $\epsilon_0 < -U/2, \epsilon_0 > -U/2$ , as  $\epsilon_0$  increases,  $\epsilon_\uparrow$  increases and  $\langle n_\uparrow \rangle$  decreases,  
 223 while the decrease is not sharp due to the MZM coupling, as shown in Fig. 3(b).

224 Next we study its single-particle DOS. As shown in Fig. 3(c), we plot the spin-resolved



225 DOS, which is defined as [63]

$$S_z^{\text{block}} = \rho_{e\uparrow} - \rho_{e\downarrow} + \rho_{h\uparrow} - \rho_{h\downarrow}. \quad (22)$$

226 Here we set  $e \uparrow, h \uparrow$  components as positive (red color), and set  $e \downarrow, h \downarrow$  components as neg-  
 227 ative (blue color). This quantity also reflects the total single-particle DOS. For  $t = 0$  with-  
 228 out MZM, the DOS of doublet state is a Coulomb diamond centered at  $\epsilon_0 = -U/2$ , like  
 229 shown in experiments [4, 13]: Two electron levels  $\epsilon_{e1} = \epsilon_0, \epsilon_{e2} = \epsilon_0 + U$  and two hole levels  
 230  $\epsilon_{h1} = -\epsilon_0, \epsilon_{h2} = -\epsilon_0 - U$ , intersecting at points  $(\epsilon_0, \epsilon) = (-U, 0), (0, 0), (-U/2, U/2)$ , and  
 231  $(-U/2, -U/2)$ . As MZM is coupled to QD, the Coulomb diamond shape almost keeps, but has  
 232 two differences: First, at  $\epsilon_0 = -U/2$  the electron spin is reversed due to phase transition, see  
 233 the two electron-like levels  $\epsilon_{e1} \approx \epsilon_0, \epsilon_{e2} \approx \epsilon_0 + U$  in Fig. 3(c). Because  $\epsilon_0 = -U/2$  is the  
 234 particle-hole symmetric point, the phase transition just changes the signs of levels, and there  
 235 is not a sharp change in the total DOS spectrum. Second, the spectrum opens two gaps at  
 236  $\epsilon_0 = -U, 0$ . Inside the gaps, the zero-energy positive peak is apparent. Because the MZM cou-  
 237 ples to spin-up channel, this peak indicates the high equal-spin Andreev reflection strength,  
 238 which is a symbolic signature of the MZM [43, 63].

239 To quantitatively show the MZM signal, we calculate the weight of the zero-energy peak  
 240 presented in Fig. 3(d), which is defined as

$$W = \int_{-0.04U}^{0.04U} d\epsilon (\rho_{e\uparrow} + \rho_{h\uparrow}). \quad (23)$$

241 Because the MZM is only coupled to the spin-up channel, we only consider the DOS from  
 242  $e \uparrow, h \uparrow$  block and exclude irrelevant contributions. The weight is high at  $\epsilon_0 = -U, 0$ , but  
 243 low around  $\epsilon_0 = -U/2$ . The distinct MZM signal can also be understood from the mean-field  
 244 picture. In fact, the MZM can always induce a zero energy peak as shown in Fig. 3(c), but the  
 245 leakage strength is strongly dependent on the ratio  $t/|\epsilon_\uparrow|$ . Note that the leakage of MZM is  
 246 strong for a low  $|\epsilon_\uparrow|$  value. For  $\epsilon_0 < -U/2$ ,  $\epsilon_\uparrow = \epsilon_0 + U$  is zero at  $\epsilon_0 = -U$ . For  $\epsilon_0 > -U/2$ ,  
 247  $\epsilon_\uparrow = \epsilon_0$  is zero at  $\epsilon_0 = 0$ . Therefore, the weight is maximized at  $\epsilon_0 = -U, 0$ . If the spin-up  
 248 effective level  $\epsilon_\uparrow$  is far away from zero (e.g.  $\epsilon_0 = -U/2$ ), the MZM will be prohibited from  
 249 leaking into the QD. It indicates that when experimentally probing MZM, even if the MZM  
 250 actually exists, its signal may be subtle because it is weakened by a high QD energy level  $|\epsilon_\uparrow|$ .

## 251 4 Phase transition with Zeeman term

252 Above we study the phase transition without considering the Zeeman term. In fact, this Zee-  
 253 man term should be **included**, because the nontrivial phase of topological superconductors  
 254 and MZM are usually induced by a magnetic field [18, 19], or **by** an exchange coupling from  
 255 a magnetic QD [8, 9]. The magnetic direction is approximately parallel to the MZM coupling  
 256 channel spin up [43, 44]. Below we study the case with a Zeeman term, which is always set  
 257 as  $V_Z = 0.06U$ . By involving the practical Zeeman term, the phase transition features become  
 258 remarkable and can be used to understand MZM-related experiments.

259 As the Zeeman term is involved, when  $t = 0$ , the degenerate doublet GS is destroyed to  
 260 a spin-polarized GS by the Zeeman term, where the **energies** of the spin-up and spin-down  
 261 states are split by  $2V_Z$ . The phase diagram versus  $\epsilon_0$  and  $t$  is shown as Fig. 4(a): Basically,  
 262 the GS is spin-up for a high  $\epsilon_0$ , and is spin-down for a low  $\epsilon_0$ . However, the phase transition  
 263 with  $V_Z \neq 0$  does not happen at the particle-hole symmetry point  $\epsilon_0 = -U/2$ .

264 To understand this feature, we also use the mean-field picture Figs. 4(b, c). The spin-  
 265 dependent effective energy levels are  $\epsilon_\uparrow = \epsilon_0 + \langle n_\downarrow \rangle U - V_Z$  and  $\epsilon_\downarrow = \epsilon_0 + \langle n_\uparrow \rangle U + V_Z$ . When

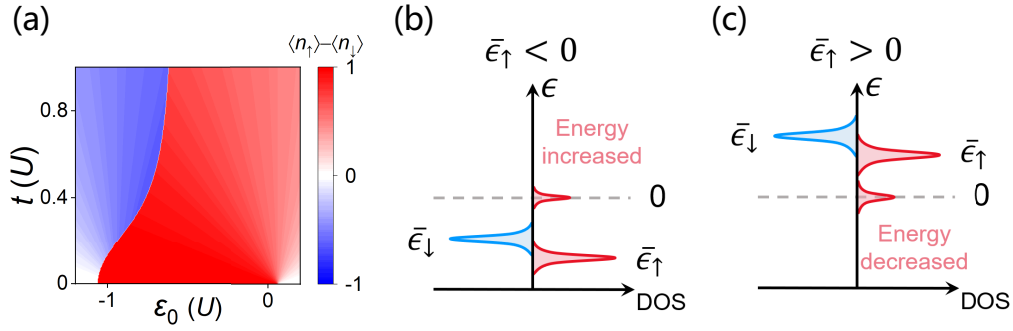


Figure 4: (a) The phase diagram versus intra-dot energy level  $\epsilon_0$  and MZM coupling strength  $t$  for  $V_Z = 0.06U$ . Here we plot  $\langle n_\uparrow \rangle - \langle n_\downarrow \rangle$  to show the spin polarization. (b, c) The mean-field picture for the phase transition. Without the coupling of MZM, spin  $\uparrow$  and  $\downarrow$  have different average energy levels  $\bar{\epsilon}_\uparrow = \epsilon_0 + U/2 - V_Z$ ,  $\bar{\epsilon}_\downarrow = \epsilon_0 + U/2 + V_Z$ .  $\bar{\epsilon}_\uparrow < \bar{\epsilon}_\downarrow$  causes a spin-up GS. The MZM effectively lifts (decreases) the spin- $\uparrow$  energy for  $\bar{\epsilon}_\uparrow < 0$  ( $\bar{\epsilon}_\uparrow > 0$ ). When the effective spin- $\uparrow$  energy is lifted over spin- $\downarrow$  energy, the GS changes from spin-up to spin-down.

266 MZM is absent  $t = 0$ , by substituting  $(\langle n_\uparrow \rangle, \langle n_\downarrow \rangle) = (1, 0), (0, 1)$  and taking the average, one  
 267 finds  $\bar{\epsilon}_\uparrow = \epsilon_0 + U/2 - V_Z$ ,  $\bar{\epsilon}_\downarrow = \epsilon_0 + U/2 + V_Z$  that determine GS spin. The relation  $\bar{\epsilon}_\uparrow < \bar{\epsilon}_\downarrow$   
 268 destroys the degeneracy of doublet GS to spin-up GS. The MZM can change the spin-up GS  
 269 to spin-down **through** the leakage effect: As shown in Figs. 4(b, c), the MZM effectively lifts  
 270 (reduces) the energy of spin-up state towards 0 for  $\bar{\epsilon}_\uparrow < 0$  ( $\bar{\epsilon}_\uparrow > 0$ ). Thus, if the effective  
 271 energy of spin up is lifted to higher than  $\bar{\epsilon}_\downarrow$ , the GS will be changed to the spin-down state.  
 272 This demands two conditions: First,  $\bar{\epsilon}_\downarrow < 0$  (which sufficiently satisfies  $\bar{\epsilon}_\uparrow < 0$ ) because the  
 273 effective energy of spin up is at most raised to 0. Second, the QD-MZM coupling  $t$  should  
 274 be high enough, so that the spin-up energy can be lifted to overcome the energy difference  
 275  $\bar{\epsilon}_\downarrow - \bar{\epsilon}_\uparrow = 2V_Z$ . Note that for a low  $\epsilon_0$ , the ratio  $|\bar{\epsilon}_\downarrow - \bar{\epsilon}_\uparrow|/|\bar{\epsilon}_\downarrow|$  is low, and the phase transition can  
 276 happen for a relatively low QD-MZM coupling  $t$ , as shown in Fig. 4(a). The GS transition line  
 277 is vertical without the Zeeman energy [Fig. 2(a)], which means that the GS can only change  
 278 by regulating the intra-dot energy level  $\epsilon_0$ . But the Zeeman term changes the GS transition  
 279 line to be oblique [Fig. 4(a)], and it becomes possible to also change the GS via just increasing  
 280 QD-MZM coupling strength  $t$ , which is studied later.

281 The representative phase transition versus intra-dot energy level  $\epsilon_0$  is summarized in Fig.  
 282 5, fixing  $t = 0.1U$ . Compared to the  $V_Z = 0$  case Fig. 3(a), the energy of spin-up state  $\epsilon_{1,-}$  and  
 283 spin-down state  $\epsilon_{3,-}$  is respectively reduced and lifted by about  $V_Z$ . This leads to the change  
 284 of critical intra-dot energy level from  $\epsilon_0 = -U/2$  to  $\epsilon_0 = \epsilon_c < -U/2$  [Fig. 5(a)]. In Fig. 5(b),  
 285 the occupation number  $\langle n_\downarrow \rangle$  is suddenly changed from 1 to 0 at  $\epsilon_0 = \epsilon_c$ . But the change of  
 286  $\langle n_\uparrow \rangle$  is not remarkable, because the critical energy level  $\epsilon_c$  is about  $-U$  and GS tends to be a  
 287 double occupation singlet state  $\frac{1}{\sqrt{2}}(|\uparrow\downarrow\rangle - |\downarrow\uparrow\rangle)$  and spin-up level always tends to be occupied.

288 With the Zeeman term, the single-particle DOS versus  $\epsilon_0$  still behaves the Coulomb dia-  
 289 mond feature, as shown in Fig. 5(c). Unlike the phase transition and spin reversion in Fig.  
 290 3(c), here the spin keeps in the range  $\epsilon_0 > \epsilon_c \approx -U$  [see the spectral lines with positive slopes]  
 291 indicating the large parameter range of the spin-up GS. When the phase transition happens  
 292 ( $\epsilon_0 = \epsilon_c$ ), the spin-down states intersect at zero energy. Meanwhile, the spin-resolved DOS  
 293 peaks with nonzero energy have the energy unchanged but spin sign reversed. Notably, the  
 294 zero-energy peak of MZM is subtle on the right of  $\epsilon_c$ , but is obvious on the left. This is because  
 295  $\epsilon_\uparrow = \epsilon_c + U \approx 0$  on the left suddenly changes to  $\epsilon_\uparrow = \epsilon_c \approx -U$  on the right. The sharp increase  
 296 of  $|\epsilon_\uparrow|$  causes the sharp decrease of MZM leakage, which is quantitatively shown in the weight  
 297  $W$  [Fig. 5(d)]. This can be analogized to the weight transitions of Andreev bound states in

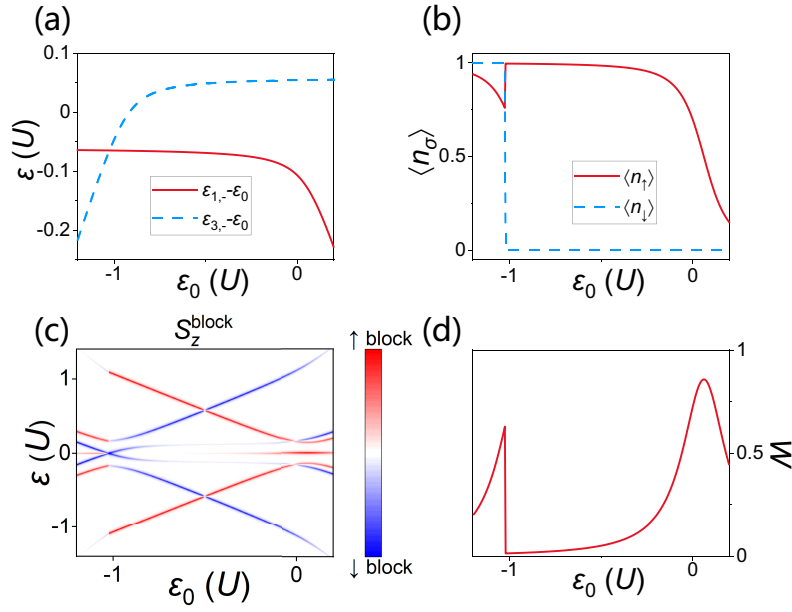


Figure 5: Phase transition of GS versus intra-dot energy level  $\epsilon_0$  for  $V_Z = 0.06U$ . (a) Energy comparison of spin-up and spin-down states  $\epsilon_{1,-}$  and  $\epsilon_{3,-}$ .  $\epsilon_0$  is **subtracted** for clarity. (b) The occupation numbers  $\langle n_\uparrow \rangle$ ,  $\langle n_\downarrow \rangle$  of GS. (c) The spin-resolved single-particle DOS. (d) The weight of zero-energy spin-up DOS. In these figures (a-d), the QD-MZM coupling strength  $t = 0.1U$ .

298 QD-conventional superconductor system in Ref. [2]. In Fig. 5(d), with the increase of  $\epsilon_0$  from  
 299  $\epsilon_c$ , the weight gradually becomes apparent due to the decreased  $|\epsilon_\uparrow|$ , and it has a large value  
 300 for a high energy level  $\epsilon_0$ , like the  $V_Z = 0$  case Fig. 3(d). Correspondingly, in Fig. 5(c) as  $\epsilon_0$  is  
 301 further increased to about 0, the MZM signal becomes apparent again. These results are similar  
 302 to the experimental result by Mourik et al. in a Majorana nanowire (their Fig. 3A) [23]: A QD  
 303 region is formed by a section of nanowire with the energy level controlled by the gate voltage,  
 304 which corresponds to  $-\epsilon_0$  in our work. When regulating the gate voltage, the nonzero-energy  
 305 states cross at zero energy. Around the crossing, the zero energy signature seems missing on  
 306 one side, but becomes apparent on the other side. Also, on the signature-missing side, as gate  
 307 voltage is turned away from the crossing point, the zero energy peak gradually appears [23].  
 308 The zero-energy crossing, the sharp change of MZM signal, and the reemergence of zero-bias  
 309 peak are very consistent with our results Figs. 5(c, d). Our theoretical analysis can provide  
 310 such kind of experiments with a potential understanding from the perspective of QD phase  
 311 transitions, with MZM already existed. They also indicate that even if the zero-bias peak is  
 312 absent, we can not definitely judge that the MZM is absent.

313 As shown by the phase diagram Fig. 4(a), the phase transition can also **occur** by just  
 314 increasing QD-MZM coupling strength  $t$ . For a fixed intra-dot energy level  $\epsilon_0 = -0.9U$ , in-  
 315 creasing  $t$  from zero to the critical value  $t_c$  indeed leads to the phase transition. As shown  
 316 in Fig. 6(a), the **energies** of spin-up and spin-down states are split by about  $2V_Z$  at  $t \rightarrow 0$ ,  
 317 indicating a spin-up GS. Along with the increase of  $t$ , the **energies** of two states both decrease  
 318 but the spin-down energy  $\epsilon_{3,-}$  decreases faster. When  $t$  reaches  $t_c$ ,  $\epsilon_{3,-}$  becomes lower than  
 319  $\epsilon_{1,-}$  and the GS becomes the spin-down state  $\psi_{3,-}$ . In comparison, for  $V_Z = 0$ , when  $t = 0$ ,  
 320  $\epsilon_{3,-} = \epsilon_{1,-} = \epsilon_0$  are degenerate in the doublet region. For the same  $\epsilon_0 = -0.9U$ , due to the  
 321 faster decrease of  $\epsilon_{3,-}$  versus  $t$ , the GS becomes spin-down state as long as  $t \neq 0$ , consistent  
 322 with the  $V_Z = 0$  phase diagram Fig. 2(a).

323 The occupation numbers versus  $t$  in Fig. 6(b) also show the phase transition. Along

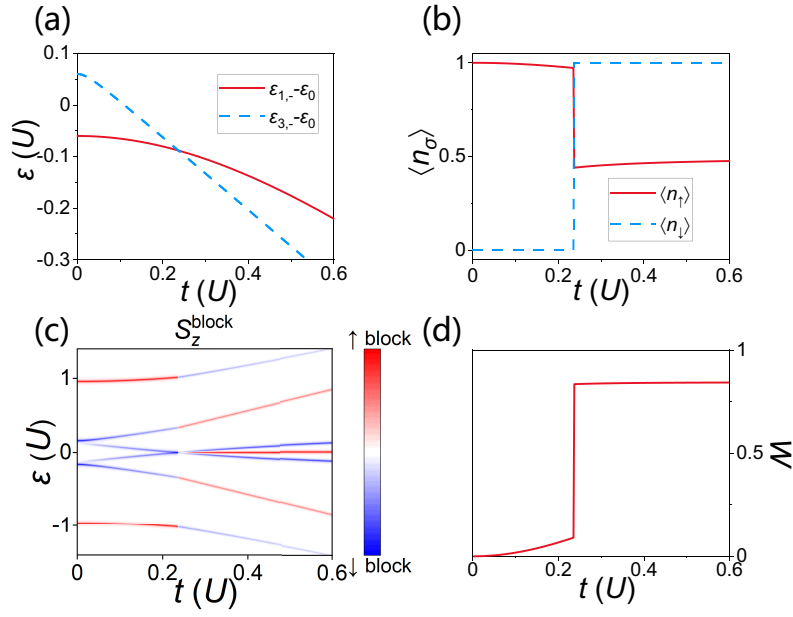


Figure 6: Phase transition of GS versus QD-MZM coupling strength  $t$  for  $V_Z = 0.06U$ . (a) Energy comparison of spin-up and spin-down states  $\epsilon_{1,-}$  and  $\epsilon_{3,-}$ .  $\epsilon_0$  is **subtracted** for clarity. (b) The occupation numbers  $\langle n_\uparrow \rangle$ ,  $\langle n_\downarrow \rangle$  of GS. (c) The spin-resolved single-particle DOS. (d) The weight of zero-energy spin-up DOS. In these figures (a-d), the intra-dot energy level  $\epsilon_0 = -0.9U$ .

324 with the increase of  $t$  and phase transition happens at  $t = t_c$ ,  $\langle n_\downarrow \rangle$  changes from 0 to 1,  
 325  $\epsilon_\uparrow = \epsilon_0 + \langle n_\downarrow \rangle U$  changes from  $-0.9U$  to  $0.1U$ . Because of the coupling of the MZM, the occu-  
 326 pation number  $\langle n_\uparrow \rangle$  always tends to be 0.5 as  $t$  increases, for both  $t < t_c$  and  $t > t_c$ . For  $t < t_c$   
 327 and  $\epsilon_\uparrow = -0.9U$ , the spin-up channel is almost occupied with  $\langle n_\uparrow \rangle \approx 1$ . After phase transition  
 328  $t > t_c$ ,  $\epsilon_\uparrow = 0.1U$  is much smaller than the QD-MZM coupling  $t$ , so the MZM leakage turns  
 329  $\langle n_\uparrow \rangle$  to be about 0.5. Therefore, the evolved state of **the** QD for a large  $t$  is almost equally  
 330 contributed by a spin-down state  $\frac{1}{\sqrt{2}}|\downarrow\rangle$  and a double occupation singlet state  $\frac{1}{2}(|\uparrow\downarrow\rangle - |\downarrow\uparrow\rangle)$ .  
 331 The spin-resolved single-particle DOS of the GS is also shown in Fig. 6(c). Like the phase transi-  
 332 tion versus  $\epsilon_0$ , the spin-down levels cross at zero energy at transition point  $t = t_c$ , and the  
 333 nonzero-energy peaks have energy unchanged but spin sign reversed at  $t = t_c$ . The zero en-  
 334 ergy peak, which reflects the leakage of MZM, is subtle when  $t < t_c$  but apparent when  $t > t_c$ ,  
 335 because  $|\epsilon_\uparrow|$  is decreased from  $0.9U$  to  $0.1U$ . The weight in Fig. 6(d) gives the quantitative  
 336 description of the emergence of strong zero energy peak.

337 The MZM *becomes apparent only when the coupling strength  $t$  reaches a critical value  $t_c$  that*  
 338 *leads to the phase transition.* Our theoretical result could provide an understanding of MZM-  
 339 related transport measurements. It is consistent with the recent experimental work by Fan et  
 340 al. in the platform of iron-based superconductor [9], which is believed as one of condensed  
 341 matter systems to realize MZMs [9, 30, 31]. Some adatoms are deposited on the surface of  
 342 the superconductor and create nearby MZMs via their exchange coupling. The adatom can be  
 343 viewed as a QD, and its coupling strength to the MZM is controlled by the distance between the  
 344 adatom and the superconductor surface. As the adatom is pushed toward the superconductor,  
 345 the coupling strength increases and the nonzero energy states cross, and the MZM zero-energy  
 346 peak appears after this crossing [9].

347 In phase transitions versus both intra-dot energy level  $\epsilon_0$  and QD-MZM coupling strength  
 348  $t$ , the single-particle DOS Figs. 5(c), 6(c) exhibit energy level crossing at the transition point  
 349  $\epsilon_c, t_c$ . Also, after the phase transition, the MZM zero-energy peak becomes apparent, which

350 may be mistakenly regarded as the emergence of MZM itself: Similarly, when researchers  
 351 regulate topological transition and induce the appearance of MZM, *the energy gap usually*  
 352 *closes, and reopens with a new zero-energy peak* indicating the MZM emergence [16,33]. Here,  
 353 we show that even when MZM already exists, the phase transition of QD leads to *the same*  
 354 *feature* as that of topological transition. Therefore, the MZM does not necessarily induce a  
 355 zero-bias peak. Even if the zero-bias peak does not exist, one can not definitely judge that the  
 356 MZM is nonexistent.

## 357 5 Conclusion

358 In summary, the phase transitions in QD-MZM coupling systems are investigated. The phase  
 359 diagrams without and with Zeeman terms are both given, showing the transition lines. The  
 360 phase transitions can happen via regulating the intra-dot energy level or QD-MZM coupling  
 361 strength. Along with these phase transitions, the occupation numbers and single-particle DOS  
 362 are studied. The transition features can be understood by the mean-field picture. Our study  
 363 not only provides an analogy to QD-superconductor phase transitions, but also offers an un-  
 364 derstanding on MZM-probing experiments.

## 365 Acknowledgements

366 We are grateful to Yu-Chen Zhuang and Yi-Xin Dai for fruitful discussions.

367 **Funding information** This work was financially supported by the National Key R and D Pro-  
 368 gram of China (Grant No. 2024YFA1409002), the National Natural Science Foundation of  
 369 China (Grants No. 12374034 and No. 11921005), and the Innovation Program for Quan-  
 370 tum Science and Technology (Grant No. 2021ZD0302403). The computational resources are  
 371 supported by High-performance Computing Platform of Peking University.

## 372 A The role of normal lead

373 In Eq. (19), the normal lead just gives a finite broadening to the states, which may seem to be  
 374 just a complication in computation. However, this broadening is essential **for demonstrating**  
 375 the change of MZM weight and the inspiration to experimental detections.

376 In Fig. 7(a), we plot the energy of eigenstates versus  $\epsilon_0$ . This corresponds to Fig. 5(c) and  
 377 can be obtained no matter the normal lead coupling is present or not. For clarity, we also show  
 378 Fig. 5(c) again in Fig. 7(b), which can be obtained only when the normal lead is coupled to  
 379 **the** QD. Indeed, the **eigenenergies** Fig. 7(a) **are** consistent with the spin-resolved DOS Fig.  
 380 7(b). However, compared to Fig. 7(b), Fig. 7(a) lacks the weight information: In Fig. 7(a),  
 381 one finds that a zero-energy state always exists. Only in Fig. 7(b) when the QD couples to  
 382 normal lead, one can **identify** that the MZM weight changes violently versus  $\epsilon_0$ , and notice  
 383 that the phase transition plays an important role on the visibility of MZM signal.

384 Therefore, the coupling of normal lead provides the weight information, which can not  
 385 be obtained by just solving the eigenenergy. On the other hand, the normal lead is usually  
 386 demanded in MZM detections, thus introducing the lead is natural and consistent with exper-  
 387 imental conditions.

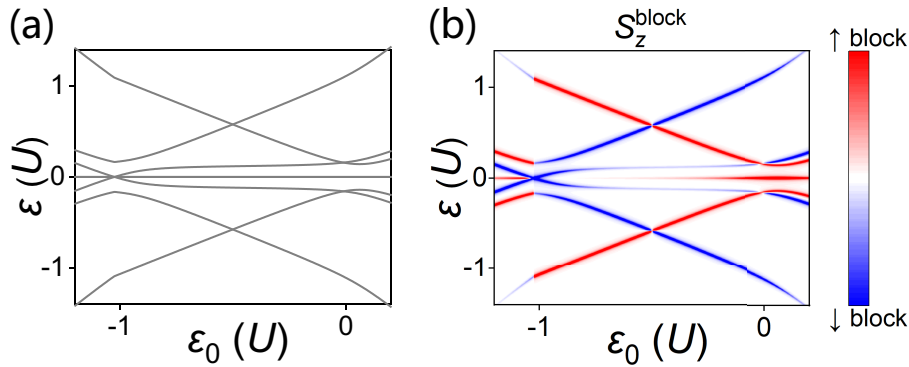


Figure 7: (a) The energy of states versus  $\epsilon_0$ . (b) In the presence of a normal lead, the spin-resolved single-particle DOS versus  $\epsilon_0$  (the same data as Fig. 5(c), but the colorbar is adjusted for clarity).

## References

- 388
- 389 [1] E. Vecino, A. Martín-Rodero and A. L. Yeyati, *Josephson current through a correlated quan-*  
 390 *tum level: Andreev states and  $\pi$  junction behavior*, Phys. Rev. B **68**(3), 035105 (2003),  
 391 doi:[10.1103/PhysRevB.68.035105](https://doi.org/10.1103/PhysRevB.68.035105).
- 392 [2] R. S. Deacon, Y. Tanaka, A. Oiwa, R. Sakano, K. Yoshida, K. Shibata, K. Hi-  
 393 rakawa and S. Tarucha, *Tunneling Spectroscopy of Andreev Energy Levels in a Quan-*  
 394 *tum Dot Coupled to a Superconductor*, Phys. Rev. Lett. **104**(7), 076805 (2010),  
 395 doi:[10.1103/PhysRevLett.104.076805](https://doi.org/10.1103/PhysRevLett.104.076805).
- 396 [3] W. Chang, V. E. Manucharyan, T. S. Jespersen, J. Nygård and C. M. Marcus, *Tunneling*  
 397 *Spectroscopy of Quasiparticle Bound States in a Spinful Josephson Junction*, Phys. Rev. Lett.  
 398 **110**(21), 217005 (2013), doi:[10.1103/PhysRevLett.110.217005](https://doi.org/10.1103/PhysRevLett.110.217005).
- 399 [4] E. J. H. Lee, X. Jiang, M. Houzet, R. Aguado, C. M. Lieber and S. De Franceschi, *Spin-*  
 400 *resolved Andreev levels and parity crossings in hybrid superconductor–semiconductor nanos-*  
 401 *tructures*, Nature Nanotech **9**(1), 79 (2014), doi:[10.1038/nnano.2013.267](https://doi.org/10.1038/nnano.2013.267).
- 402 [5] E. J. H. Lee, X. Jiang, R. Žitko, R. Aguado, C. M. Lieber and S. De Franceschi, *Scaling of*  
 403 *subgap excitations in a superconductor-semiconductor nanowire quantum dot*, Phys. Rev.  
 404 B **95**(18), 180502 (2017), doi:[10.1103/PhysRevB.95.180502](https://doi.org/10.1103/PhysRevB.95.180502).
- 405 [6] M. Valentini, F. Peñaranda, A. Hofmann, M. Brauns, R. Hauschild, P. Krogstrup, P. San-  
 406 Jose, E. Prada, R. Aguado and G. Katsaros, *Nontopological zero-bias peaks in full-*  
 407 *shell nanowires induced by flux-tunable Andreev states*, Science **373**(6550), 82 (2021),  
 408 doi:[10.1126/science.abf1513](https://doi.org/10.1126/science.abf1513).
- 409 [7] A. Bargerbos, M. Pita-Vidal, R. Žitko, J. Ávila, L. J. Splitthoff, L. Grünhaupt, J. J. Wesdorp,  
 410 C. K. Andersen, Y. Liu, L. P. Kouwenhoven, R. Aguado, A. Kou *et al.*, *Singlet-Doublet*  
 411 *Transitions of a Quantum Dot Josephson Junction Detected in a Transmon Circuit*, PRX  
 412 Quantum **3**(3), 030311 (2022), doi:[10.1103/PRXQuantum.3.030311](https://doi.org/10.1103/PRXQuantum.3.030311).
- 413 [8] K. Jiang, X. Dai and Z. Wang, *Quantum Anomalous Vortex and Majorana Zero*  
 414 *Mode in Iron-Based Superconductor Fe(Te,Se)*, Phys. Rev. X **9**(1), 011033 (2019),  
 415 doi:[10.1103/PhysRevX.9.011033](https://doi.org/10.1103/PhysRevX.9.011033).

- 416 [9] P. Fan, F. Yang, G. Qian, H. Chen, Y.-Y. Zhang, G. Li, Z. Huang, Y. Xing, L. Kong, W. Liu,  
417 K. Jiang, C. Shen *et al.*, *Observation of magnetic adatom-induced Majorana vortex and*  
418 *its hybridization with field-induced Majorana vortex in an iron-based superconductor*, *Nat*  
419 *Commun* **12**(1), 1348 (2021), doi:[10.1038/s41467-021-21646-x](https://doi.org/10.1038/s41467-021-21646-x).
- 420 [10] C.-K. Chiu and Z. Wang, *Yu-Shiba-Rusinov States in a Superconductor with Topological Z<sub>2</sub>*  
421 *Bands*, *Phys. Rev. Lett.* **128**(23), 237001 (2022), doi:[10.1103/PhysRevLett.128.237001](https://doi.org/10.1103/PhysRevLett.128.237001).
- 422 [11] J. Bauer, A. Oguri and A. C. Hewson, *Spectral properties of locally correlated electrons in*  
423 *a Bardeen–Cooper–Schrieffer superconductor*, *J. Phys.: Condens. Matter* **19**(48), 486211  
424 (2007), doi:[10.1088/0953-8984/19/48/486211](https://doi.org/10.1088/0953-8984/19/48/486211).
- 425 [12] T. Meng, S. Florens and P. Simon, *Self-consistent description of Andreev bound*  
426 *states in Josephson quantum dot devices*, *Phys. Rev. B* **79**(22), 224521 (2009),  
427 doi:[10.1103/PhysRevB.79.224521](https://doi.org/10.1103/PhysRevB.79.224521).
- 428 [13] J. A. Van Dam, Y. V. Nazarov, E. P. A. M. Bakkers, S. De Franceschi and L. P. Kouwen-  
429 hoven, *Supercurrent reversal in quantum dots*, *Nature* **442**(7103), 667 (2006),  
430 doi:[10.1038/nature05018](https://doi.org/10.1038/nature05018).
- 431 [14] Q. Cheng and Q.-F. Sun, *Switch effect and 0- $\pi$  transition in Ising superconductor Josephson*  
432 *junctions*, *Phys. Rev. B* **99**(18), 184507 (2019), doi:[10.1103/PhysRevB.99.184507](https://doi.org/10.1103/PhysRevB.99.184507).
- 433 [15] S. R. Elliott and M. Franz, *Colloquium : Majorana fermions in nuclear, particle, and solid-*  
434 *state physics*, *Rev. Mod. Phys.* **87**(1), 137 (2015), doi:[10.1103/RevModPhys.87.137](https://doi.org/10.1103/RevModPhys.87.137).
- 435 [16] E. Prada, P. San-Jose, M. W. A. De Moor, A. Geresdi, E. J. H. Lee, J. Klinovaja, D. Loss,  
436 J. Nygård, R. Aguado and L. P. Kouwenhoven, *From Andreev to Majorana bound states*  
437 *in hybrid superconductor–semiconductor nanowires*, *Nat Rev Phys* **2**(10), 575 (2020),  
438 doi:[10.1038/s42254-020-0228-y](https://doi.org/10.1038/s42254-020-0228-y).
- 439 [17] A. Y. Kitaev, *Unpaired Majorana fermions in quantum wires*, *Phys.-Usp.* **44**(10S), 131  
440 (2001), doi:[10.1070/1063-7869/44/10S/S29](https://doi.org/10.1070/1063-7869/44/10S/S29).
- 441 [18] Y. Oreg, G. Refael and F. Von Oppen, *Helical Liquids and Majorana Bound*  
442 *States in Quantum Wires*, *Phys. Rev. Lett.* **105**(17), 177002 (2010),  
443 doi:[10.1103/PhysRevLett.105.177002](https://doi.org/10.1103/PhysRevLett.105.177002).
- 444 [19] R. M. Lutchyn, J. D. Sau and S. Das Sarma, *Majorana Fermions and a Topological Phase*  
445 *Transition in Semiconductor-Superconductor Heterostructures*, *Phys. Rev. Lett.* **105**(7),  
446 077001 (2010), doi:[10.1103/PhysRevLett.105.077001](https://doi.org/10.1103/PhysRevLett.105.077001).
- 447 [20] R. M. Lutchyn, E. P. A. M. Bakkers, L. P. Kouwenhoven, P. Krogstrup, C. M. Marcus and  
448 Y. Oreg, *Majorana zero modes in superconductor–semiconductor heterostructures*, *Nat Rev*  
449 *Mater* **3**(5), 52 (2018), doi:[10.1038/s41578-018-0003-1](https://doi.org/10.1038/s41578-018-0003-1).
- 450 [21] M. T. Deng, S. Vaitiekėnas, E. B. Hansen, J. Danon, M. Leijnse, K. Flensberg, J. Nygård,  
451 P. Krogstrup and C. M. Marcus, *Majorana bound state in a coupled quantum-dot hybrid-*  
452 *nanowire system*, *Science* **354**(6319), 1557 (2016), doi:[10.1126/science.aaf3961](https://doi.org/10.1126/science.aaf3961).
- 453 [22] E. Prada, R. Aguado and P. San-Jose, *Measuring Majorana nonlocality and*  
454 *spin structure with a quantum dot*, *Phys. Rev. B* **96**(8), 085418 (2017),  
455 doi:[10.1103/PhysRevB.96.085418](https://doi.org/10.1103/PhysRevB.96.085418).

- 456 [23] V. Mourik, K. Zuo, S. M. Frolov, S. R. Plissard, E. P. A. M. Bakkers and L. P. Kouwenhoven,  
457 *Signatures of Majorana Fermions in Hybrid Superconductor-Semiconductor Nanowire De-*  
458 *VICES*, *Science* **336**(6084), 1003 (2012), doi:[10.1126/science.1222360](https://doi.org/10.1126/science.1222360).
- 459 [24] J. Li, H. Chen, I. K. Drozdov, A. Yazdani, B. A. Bernevig and A. H. MacDonald, *Topological*  
460 *superconductivity induced by ferromagnetic metal chains*, *Phys. Rev. B* **90**(23), 235433  
461 (2014), doi:[10.1103/PhysRevB.90.235433](https://doi.org/10.1103/PhysRevB.90.235433).
- 462 [25] S. Nadj-Perge, I. K. Drozdov, J. Li, H. Chen, S. Jeon, J. Seo, A. H. MacDonald, B. A.  
463 Bernevig and A. Yazdani, *Observation of Majorana fermions in ferromagnetic atomic chains*  
464 *on a superconductor*, *Science* **346**(6209), 602 (2014), doi:[10.1126/science.1259327](https://doi.org/10.1126/science.1259327).
- 465 [26] S. Jeon, Y. Xie, J. Li, Z. Wang, B. A. Bernevig and A. Yazdani, *Distinguishing a Ma-*  
466 *ajorana zero mode using spin-resolved measurements*, *Science* **358**(6364), 772 (2017),  
467 doi:[10.1126/science.aan3670](https://doi.org/10.1126/science.aan3670).
- 468 [27] B. Jäck, Y. Xie, J. Li, S. Jeon, B. A. Bernevig and A. Yazdani, *Observation of a Majorana*  
469 *zero mode in a topologically protected edge channel*, *Science* **364**(6447), 1255 (2019),  
470 doi:[10.1126/science.aax1444](https://doi.org/10.1126/science.aax1444).
- 471 [28] J.-P. Xu, M.-X. Wang, Z. L. Liu, J.-F. Ge, X. Yang, C. Liu, Z. A. Xu, D. Guan, C. L.  
472 Gao, D. Qian, Y. Liu, Q.-H. Wang *et al.*, *Experimental Detection of a Majorana*  
473 *Mode in the core of a Magnetic Vortex inside a Topological Insulator-Superconductor*  
474 *Bi<sub>2</sub>Te<sub>3</sub> / NbSe<sub>2</sub> Heterostructure*, *Phys. Rev. Lett.* **114**(1), 017001 (2015),  
475 doi:[10.1103/PhysRevLett.114.017001](https://doi.org/10.1103/PhysRevLett.114.017001).
- 476 [29] H.-H. Sun, K.-W. Zhang, L.-H. Hu, C. Li, G.-Y. Wang, H.-Y. Ma, Z.-A. Xu, C.-L. Gao, D.-D.  
477 Guan, Y.-Y. Li, C. Liu, D. Qian *et al.*, *Majorana Zero Mode Detected with Spin Selective*  
478 *Andreev Reflection in the Vortex of a Topological Superconductor*, *Phys. Rev. Lett.* **116**(25),  
479 257003 (2016), doi:[10.1103/PhysRevLett.116.257003](https://doi.org/10.1103/PhysRevLett.116.257003).
- 480 [30] D. Wang, L. Kong, P. Fan, H. Chen, S. Zhu, W. Liu, L. Cao, Y. Sun, S. Du, J. Schneeloch,  
481 R. Zhong, G. Gu *et al.*, *Evidence for Majorana bound states in an iron-based superconductor*,  
482 *Science* **362**(6412), 333 (2018), doi:[10.1126/science.aao1797](https://doi.org/10.1126/science.aao1797).
- 483 [31] S. Zhu, L. Kong, L. Cao, H. Chen, M. Papaj, S. Du, Y. Xing, W. Liu, D. Wang,  
484 C. Shen, F. Yang, J. Schneeloch *et al.*, *Nearly quantized conductance plateau of vor-*  
485 *tex zero mode in an iron-based superconductor*, *Science* **367**(6474), 189 (2020),  
486 doi:[10.1126/science.aax0274](https://doi.org/10.1126/science.aax0274).
- 487 [32] M. Serina, D. Loss and J. Klinovaja, *Boundary spin polarization as a robust signature of a*  
488 *topological phase transition in Majorana nanowires*, *Phys. Rev. B* **98**(3), 035419 (2018),  
489 doi:[10.1103/PhysRevB.98.035419](https://doi.org/10.1103/PhysRevB.98.035419).
- 490 [33] Y. Zhuang and Q.-F. Sun, *Anomalous photon-assisted tunneling in periodically driven Ma-*  
491 *ajorana nanowires and BCS charge measurement*, *Phys. Rev. B* **105**(16), 165148 (2022),  
492 doi:[10.1103/PhysRevB.105.165148](https://doi.org/10.1103/PhysRevB.105.165148).
- 493 [34] M. Aghaee, A. Akkala, Z. Alam, R. Ali, A. Alcaraz Ramirez, M. Andrzejczuk, A. E. An-  
494 tipov, P. Aseev, M. Astafev, B. Bauer, J. Becker, S. Boddapati *et al.*, *InAs-Al hybrid*  
495 *devices passing the topological gap protocol*, *Phys. Rev. B* **107**(24), 245423 (2023),  
496 doi:[10.1103/PhysRevB.107.245423](https://doi.org/10.1103/PhysRevB.107.245423).
- 497 [35] X.-F. Chen, W. Luo, T.-F. Fang, Y. Paltiel, O. Millo, A.-M. Guo and Q.-F. Sun, *Topologically*  
498 *nontrivial and trivial zero modes in chiral molecules*, *Phys. Rev. B* **108**(3), 035401 (2023),  
499 doi:[10.1103/PhysRevB.108.035401](https://doi.org/10.1103/PhysRevB.108.035401).



- 500 [36] X. Zhang, C.-M. Miao, Q.-F. Sun and Y.-T. Zhang, *Nonendpoint Majorana bound*  
501 *states in an extended Kitaev chain*, Phys. Rev. B **109**(20), 205119 (2024),  
502 doi:[10.1103/PhysRevB.109.205119](https://doi.org/10.1103/PhysRevB.109.205119).
- 503 [37] F. Peñaranda, R. Aguado, E. Prada and P. San-Jose, *Majorana bound states in encapsulated*  
504 *bilayer graphene*, SciPost Phys. **14**(4), 075 (2023), doi:[10.21468/SciPostPhys.14.4.075](https://doi.org/10.21468/SciPostPhys.14.4.075).
- 505 [38] A. Kitaev, *Fault-tolerant quantum computation by anyons*, Annals of Physics **303**(1), 2  
506 (2003), doi:[10.1016/S0003-4916\(02\)00018-0](https://doi.org/10.1016/S0003-4916(02)00018-0).
- 507 [39] C. Nayak, S. H. Simon, A. Stern, M. Freedman and S. Das Sarma, *Non-Abelian*  
508 *anyons and topological quantum computation*, Rev. Mod. Phys. **80**(3), 1083 (2008),  
509 doi:[10.1103/RevModPhys.80.1083](https://doi.org/10.1103/RevModPhys.80.1083).
- 510 [40] Y.-F. Zhou, Z. Hou and Q.-F. Sun, *Non-Abelian operation on chiral Majorana fermions by*  
511 *quantum dots*, Phys. Rev. B **99**(19), 195137 (2019), doi:[10.1103/PhysRevB.99.195137](https://doi.org/10.1103/PhysRevB.99.195137).
- 512 [41] Q. Yan, Y.-F. Zhou and Q.-F. Sun, *Electrically tunable chiral Majorana edge modes in quan-*  
513 *tum anomalous Hall insulator–topological superconductor systems*, Phys. Rev. B **100**(23),  
514 235407 (2019), doi:[10.1103/PhysRevB.100.235407](https://doi.org/10.1103/PhysRevB.100.235407).
- 515 [42] K. T. Law, P. A. Lee and T. K. Ng, *Majorana Fermion Induced Resonant Andreev Reflection*,  
516 Phys. Rev. Lett. **103**(23), 237001 (2009), doi:[10.1103/PhysRevLett.103.237001](https://doi.org/10.1103/PhysRevLett.103.237001).
- 517 [43] J. J. He, T. Ng, P. A. Lee and K. Law, *Selective Equal-Spin Andreev Reflec-*  
518 *tions Induced by Majorana Fermions*, Phys. Rev. Lett. **112**(3), 037001 (2014),  
519 doi:[10.1103/PhysRevLett.112.037001](https://doi.org/10.1103/PhysRevLett.112.037001).
- 520 [44] Y. Mao and Q.-F. Sun, *Spin phase regulated spin Josephson supercur-*  
521 *rent in topological superconductor*, Phys. Rev. B **105**(18), 184511 (2022),  
522 doi:[10.1103/PhysRevB.105.184511](https://doi.org/10.1103/PhysRevB.105.184511).
- 523 [45] X. Liu, J. D. Sau and S. Das Sarma, *Universal spin-triplet superconduct-*  
524 *ing correlations of Majorana fermions*, Phys. Rev. B **92**(1), 014513 (2015),  
525 doi:[10.1103/PhysRevB.92.014513](https://doi.org/10.1103/PhysRevB.92.014513).
- 526 [46] Y. Mao and Q.-F. Sun, *Charge and spin transport through a normal lead coupled to an s*  
527 *-wave superconductor and a Majorana zero mode*, Phys. Rev. B **103**(11), 115411 (2021),  
528 doi:[10.1103/PhysRevB.103.115411](https://doi.org/10.1103/PhysRevB.103.115411).
- 529 [47] J.-X. Yin, Z. Wu, J.-H. Wang, Z.-Y. Ye, J. Gong, X.-Y. Hou, L. Shan, A. Li, X.-J. Liang, X.-X.  
530 Wu, J. Li, C.-S. Ting *et al.*, *Observation of a robust zero-energy bound state in iron-based*  
531 *superconductor Fe(Te,Se)*, Nature Phys **11**(7), 543 (2015), doi:[10.1038/nphys3371](https://doi.org/10.1038/nphys3371).
- 532 [48] D. E. Liu and H. U. Baranger, *Detecting a Majorana-fermion zero mode using a quantum*  
533 *dot*, Phys. Rev. B **84**(20), 201308 (2011), doi:[10.1103/PhysRevB.84.201308](https://doi.org/10.1103/PhysRevB.84.201308).
- 534 [49] W.-J. Gong, S.-F. Zhang, Z.-C. Li, G. Yi and Y.-S. Zheng, *Detection of a Majorana fermion*  
535 *zero mode by a T-shaped quantum-dot structure*, Phys. Rev. B **89**(24), 245413 (2014),  
536 doi:[10.1103/PhysRevB.89.245413](https://doi.org/10.1103/PhysRevB.89.245413).
- 537 [50] A. Martín-Rodero and A. Levy Yeyati, *The Andreev states of a superconducting quantum*  
538 *dot: mean field versus exact numerical results*, J. Phys.: Condens. Matter **24**(38), 385303  
539 (2012), doi:[10.1088/0953-8984/24/38/385303](https://doi.org/10.1088/0953-8984/24/38/385303).

- 540 [51] Q.-f. Sun and T.-h. Lin, *Time-dependent electron tunnelling through a quantum dot with*  
541 *Coulomb interactions*, J. Phys.: Condens. Matter **9**(23), 4875 (1997), doi:[10.1088/0953-](https://doi.org/10.1088/0953-8984/9/23/011)  
542 [8984/9/23/011](https://doi.org/10.1088/0953-8984/9/23/011).
- 543 [52] R. Seoane Souto, A. E. Feiguin, A. Martín-Rodero and A. L. Yeyati, *Transient dynamics of*  
544 *a magnetic impurity coupled to superconducting electrodes: Exact numerics versus perturba-*  
545 *tion theory*, Phys. Rev. B **104**(21), 214506 (2021), doi:[10.1103/PhysRevB.104.214506](https://doi.org/10.1103/PhysRevB.104.214506).
- 546 [53] Q.-f. Sun and X. C. Xie, *Bias-controllable intrinsic spin polarization in a quantum dot:*  
547 *Proposed scheme based on spin-orbit interaction*, Phys. Rev. B **73**(23), 235301 (2006),  
548 doi:[10.1103/PhysRevB.73.235301](https://doi.org/10.1103/PhysRevB.73.235301).
- 549 [54] L. Pavešić, M. Pita Vidal, A. Bargerbos and R. Žitko, *Impurity Knight*  
550 *shift in quantum dot Josephson junctions*, SciPost Phys. **15**(2), 070 (2023),  
551 doi:[10.21468/SciPostPhys.15.2.070](https://doi.org/10.21468/SciPostPhys.15.2.070).
- 552 [55] D. J. Clarke, *Experimentally accessible topological quality factor for wires with zero energy*  
553 *modes*, Phys. Rev. B **96**(20), 201109 (2017), doi:[10.1103/PhysRevB.96.201109](https://doi.org/10.1103/PhysRevB.96.201109).
- 554 [56] A. Golub, I. Kuzmenko and Y. Avishai, *Kondo Correlations and Majorana Bound States in a*  
555 *Metal to Quantum-Dot to Topological-Superconductor Junction*, Phys. Rev. Lett. **107**(17),  
556 176802 (2011), doi:[10.1103/PhysRevLett.107.176802](https://doi.org/10.1103/PhysRevLett.107.176802).
- 557 [57] M. Cheng, M. Becker, B. Bauer and R. M. Lutchyn, *Interplay between Kondo*  
558 *and Majorana Interactions in Quantum Dots*, Phys. Rev. X **4**(3), 031051 (2014),  
559 doi:[10.1103/PhysRevX.4.031051](https://doi.org/10.1103/PhysRevX.4.031051).
- 560 [58] R. Žitko, J. S. Lim, R. López and R. Aguado, *Shiba states and zero-bias anomalies in*  
561 *the hybrid normal-superconductor Anderson model*, Phys. Rev. B **91**(4), 045441 (2015),  
562 doi:[10.1103/PhysRevB.91.045441](https://doi.org/10.1103/PhysRevB.91.045441).
- 563 [59] Z.-q. Bao and F. Zhang, *Topological Majorana Two-Channel Kondo Effect*, Phys. Rev. Lett.  
564 **119**(18), 187701 (2017), doi:[10.1103/PhysRevLett.119.187701](https://doi.org/10.1103/PhysRevLett.119.187701).
- 565 [60] W. Long and Q.-F. Sun, *Kondo Effect Versus Magnetic Coupling in Indirectly Coupled*  
566 *Double Quantum Dots*, Commun. Theor. Phys. **54**(5), 933 (2010), doi:[10.1088/0253-](https://doi.org/10.1088/0253-6102/54/5/28)  
567 [6102/54/5/28](https://doi.org/10.1088/0253-6102/54/5/28).
- 568 [61] Q.-f. Sun, H. Guo and T.-h. Lin, *Excess Kondo Resonance in a Quantum Dot Device with*  
569 *Normal and Superconducting Leads: The Physics of Andreev-Normal Co-tunneling*, Phys.  
570 Rev. Lett. **87**(17), 176601 (2001), doi:[10.1103/PhysRevLett.87.176601](https://doi.org/10.1103/PhysRevLett.87.176601).
- 571 [62] E. Vernek, P. H. Penteado, A. C. Seridonio and J. C. Egues, *Subtle leakage of*  
572 *a Majorana mode into a quantum dot*, Phys. Rev. B **89**(16), 165314 (2014),  
573 doi:[10.1103/PhysRevB.89.165314](https://doi.org/10.1103/PhysRevB.89.165314).
- 574 [63] L.-H. Hu, C. Li, D.-H. Xu, Y. Zhou and F.-C. Zhang, *Theory of spin-selective Andreev re-*  
575 *flexion in the vortex core of a topological superconductor*, Phys. Rev. B **94**(22), 224501  
576 (2016), doi:[10.1103/PhysRevB.94.224501](https://doi.org/10.1103/PhysRevB.94.224501).